Net-Zero Scheduling of Multi-energy Building Energy Systems: A Learning-based Robust Optimization Approach with Statistical Guarantees

Yijie Yang, Graduate Student Member, IEEE, Jian Shi, Senior Member, IEEE, Dan Wang, Senior Member, IEEE, Chenye Wu, Member, IEEE, and Zhu Han, Fellow, IEEE

Abstract—Buildings produce a significant share of greenhouse gas (GHG) emissions, making homes and businesses a major factor in climate change. To address this critical challenge, this paper explores achieving net-zero emission through the carbonaware optimal scheduling of the multi-energy building integrated energy systems (BIES). We integrate advanced technologies and strategies, such as the carbon capture system (CCS), power-togas (P2G), carbon tracking, and emission allowance trading, into the traditional BIES scheduling problem. The proposed model enables accurate accounting of carbon emissions associated with building energy systems and facilitates the implementation of low-carbon operations. Furthermore, to address the challenge of accurately assessing uncertainty sets related to forecasting errors of loads, generation, and carbon intensity, we develop a learningbased robust optimization approach for BIES that is robust in the presence of uncertainty and guarantees statistical feasibility. The proposed approach comprises a shape learning stage and a shape calibration stage to generate an optimal uncertainty set that ensures favorable results from a statistical perspective. Numerical studies conducted based on both synthetic and realworld datasets have demonstrated that the approach yields up to 8.2% cost reduction, compared with conventional methods, in assisting buildings to robustly reach net-zero emissions.

Index Terms—Carbon emission; Building integrated energy system; Robust Optimization; Chance-constrained Optimization; Net-Zero Emission

NOMENCLATURE

Indices and Sets

 t/\mathcal{T} Index/set of time periods **Parameters**

s arameters

 δ_g CO₂ emission factor of gas

 η_{cap} Electricity consumed for capturing per unit CO_2

 η_{CCS} CO₂ capture efficiency of CCS η_{CC} CO₂ utilization efficiency of P2G

 η_{P2G} P2G reaction efficiency

 I_t Carbon intensity of main grid at time t

This work is partially supported by NSF ECCS-2338158, CNS-2107216, CNS-2128368, CMMI-2222810, ECCS-2302469, US Department of Transportation, Toyota. Amazon and Japan Science and Technology Agency (JST) Adopting Sustainable Partnerships for Innovative Research Ecosystem (ASPIRE) JPMJAP2326. This work is also in part supported by RGC GRF 15200321, 15201322, 15230624, RGC-CRF C5018-20G, ITC ITF-ITS/056/22MX, and PolyU 1-CDKK.

- Y. Yang and D. Wang are with the Department of Computing, The Hong Kong Polytechnic University, Hung Hom, Kowloon, Hong Kong.
- J. Shi is with the Department of Engineering Technology and the Department of Electrical and Computer Engineering, University of Houston, Houston, Texas, USA.
- C. Wu is with the School of Science and Engineering, The Chinese University of Hong Kong, Shenzhen, Guangdong, China.
- Z. Han is with the Department of Electrical and Computer Engineering at the University of Houston, Houston, TX 77004 USA, and also with the Department of Computer Science and Engineering, Kyung Hee University, Seoul, South Korea, 446-701.

$P_{c,t}^{load}$	Actual cooling load at time t				
$P_{e,t}^{load}$	Actual electrical load at time t				
$P_{a,t}^{PV}$	PV generation at time t				
$P_{h,t}^{load}$	Actual thermal load at time t				
Q_{quota}	Carbon emission quotas for the BIES				
Variables					
E_{buy}	Purchased/sold carbon allowance in carbon mar-				
	ket				
$E_{CCS,t}^{atm}$	CO ₂ emitted into the atmosphere after introduc-				
0 0 0 7	ing CCS at time t				
$E^{cs}_{CCS,t}$	CO_2 stored via CCS at time t				
$E_{CCS,t}^{P2G}$	CO_2 consumption of P2G system at time t				
$E_{CHP,t}$	Carbon emission from CHP at time t				
$E_{CSS,t}^{cap}$	CO_2 captured via CCS at time t				
$E_{GB,t}$	Carbon emission from GB at time t				
E_{real}	Total real carbon emission during the whole time				
	period T				
$E_{virtual}$	Total virtual carbon emission from the main grid				
	during the whole time period T				
$F_{CHP,t}$	Natural gas consumption of CHP/GB at time t				
$F_{g,t}^{P2G}$	Natural gas produced via P2G process at time t				
$F_{GB,t}$	Natural gas consumption of GB at time t				
$P_{e,t}^{buy}$	Power purchased from the main grid at time t				
$P_{c,t}^{AC}$	Refrigeration power of AC at time t				
$P_{c,t}^{\dot{E}C}$	Refrigeration power of EC at time t				
$P_{e,t}^{AC}$	Electricity consumption power of EC at time t				
$P_{e,t}^{ESS}$	Charged/discharged power of ESS at time t				
$P_{e,t}^{P2G}$	Electricity consumption of P2G system at t				
$P_{h,t}^{AC}$	Heat absorption power of AC at time t				
-CHD					

The cost of carbon storage

I. Introduction

Heat generation of CHP at time t

Power generation of CHP at time t

Electricity storage level at time time t

A. Motivation and Challenges

Buildings contribute significantly to carbon neutralization due to their significant energy consumption, carbon emissions, and their potential to lead in the adoption of energy-efficient technologies and renewable energy sources. For instance, nearly a third of U.S. greenhouse gas emissions are attributable to 130 million homes and commercial buildings in America, which use 40% of the nation's energy and 75% of its electricity [1]. To achieve the urgent climate goal, the existing design of building integrated energy system (BIES) needs to evolve in a climate-responsible manner to increasingly aggregate zero/low-emission energy technologies and optimize energy efficiency,

while meeting the demand of heat, power, and cooling [2], [3]. Existing research has shown that a climate-smart BIES not only serves as the energy backbone of buildings but also acts as an innovative platform for the integration of various new technologies and strategies within the building environment to cut carbon emissions. For instance, empirical findings in [4] indicated that the implementation of technologies such as photovoltaic (PV) and energy storage systems (ESSs) in BIES could potentially decrease CO₂ emissions by 20%.

Despite the potential benefits offered by BIES, its optimal scheduling is not straightforward. The first research challenge we are facing is: How to perform synergic carbon-aware coordination of on-site components and technologies while optimizing off-site electricity usage from the utility grid, to achieve net-zero emission? BIES comprises multiple on-site components, like power-to-gas (P2G) and carbon capture systems (CCS), each presenting a method to harness renewable energy and reduce carbon footprints. The coordination between these diverse technologies and the smart use of off-site, low-carbon electricity is essential. As the share of renewable energy in the grid increases, the carbon intensity of electricity fluctuates, making it crucial to schedule energy-intensive operations during times of lower carbon intensity to minimize the carbon emission of buildings.

Another major challenge is: How do we handle uncertainties inherited in BIES operations? While renewable sources such as wind and solar generation do not create any carbon emissions, their intermittent and stochastic nature poses severe challenges to BIES operation and safety. Energy prediction has thus become a key element to accurately forecast future operating conditions using historical operation data and machine learning algorithms [5]. However, all prediction models would inevitably inherit errors. The sources of uncertainty for optimal BIES design stem from load prediction, such as cooling/heating and electrical load, as well as renewable energy production [6]. The presence of the uncertainty factor may adversely affect the performance of the model [7] and challenge the practical application of deterministic methods [8]. These uncertainties should be systematically considered during the energy management decisionmaking process involved in BIES to ensure its feasibility under various operating scenarios [9].

B. Literature Review

1) Carbon capture in BIES

CCS has proven to be an effective solution for reducing CO_2 emissions by capturing carbon directly at the source. The captured carbon can then be either stored long-term in suitable sites or converted into commercially useful by-products [10].

In the building environment, post-combustion CCS, which refers to the technology that separates CO₂ from the flue gases produced after the combustion of natural gas, is considered the most feasible technique. Post-combustion CCS units can be integrated into existing natural gas combustion systems and furnaces through retrofitting, requiring minimal modifications to building infrastructure. To date, there is an extensive body of literature on the integration of carbon capture technologies within building environments. For instance, the feasibility of installing CCS at the building level has been discussed in [11] from the market assessment perspective. The design of building integrated carbon capture (BICC) for retrofitting existing mechanical systems

within buildings was discussed in detail in [12], highlighting the significant role BICC can play in offsetting carbon emissions from different types of buildings. The modeling of CCS to deploy along with energy efficiency measures and demand response to achieve zero-emission was discussed in [13]. A comparative performance assessment was conducted in [14] to evaluate the environmental and economic performance of building-level CCS over their life cycle, showcasing the great potential for building-level CCT in regions that depend on fossil fuels to generate electricity.

In practical applications, CCS for natural gas-fueled building heating systems was first deployed and tested by FortisBC Energy in a pilot program in Canada in 2017 [15]. The participants of this program included various commercial buildings, including LUSH Cosmetics Headquarters, Baptist Housing, Starlight Housing, Richmond Centre, and Richmond School District [16]. Their latest small-scale CCS installation project was at Southridge School in 2023 [17]. It was reported that the carbon capture process could help commercial customers reduce up to 5,400 kilograms of CO₂ reduction per unit per year while decreasing energy consumption by up to 10% [17]. Furthermore, commercial carbon capture products and services, such as the solutions provided by CarbonQuest [18], have been made readily available for various building types. For example, it is reported that their larger-size Distributed Carbon Capture products can be bundled together for CHP solutions to capture over 100,000 tons of CO2 in campus settings, including universities, hospitals, and multi-building complexes [19]. Meanwhile, their Building Carbon Capture products can be deployed in commercial buildings, such as offices and mixeduse buildings, to capture 500 to 16,800 tons of CO₂ per year [19]. So far, their products have been reportedly deployed in 5 locations, with its first on-site carbon capture system installed in a multifamily building located in Manhattan's Lincoln Square neighborhood in 2021 [20][21].

At the same time, countries around the world are increasingly recognizing the significance of CCT in mitigating climate change. For instance, in the United States, the 45Q Tax Credit included in the Inflation Reduction Act (IRA) provides financial incentives and facilitates the acceleration of the demonstration and deployment of CCT in commercial applications [22]. Similarly, the European Union's Innovation Fund supports the demonstration of innovative low-carbon technologies including CCS [23]. In addition, the United Kingdom, Australia, and China have also implemented specific policies and subsidies to promote CCS [24]. These measures are crucial for expediting the commercialization of CCS technologies, which are essential for attaining global climate targets.

2) Low-carbon operation of BIES

Recent studies have significantly advanced the optimization of BIES with carbon emissions taken into account by utilizing a combination of different carbon-free technologies. In the research literature, Li et al. [25] demonstrate the integration of CCS and P2G technologies into conventional energy systems, enhancing stability and addressing energy demand and renewable generation uncertainties. Xiao et al. [26] explore a multi-energy CHP-based microgrid for smart cities, incorporating a P2G facility to reduce CO₂ emissions and considering the sale and utilization of captured CO₂. A hydrogen-based framework

that combines a refined P2G system and CCS is developed in [27], offering a novel approach to energy system design. It also highlights that to tackle the concern regarding the potential lack of cost-effectiveness in CCS applications, building owners can additionally engage in carbon trading mechanisms. These mechanisms convert emission reductions into financial gains. Some countries and regions have already implemented or are in the process of integrating carbon trading into the building sector [28]. Research Gaps: While these contributions mark significant progress in tracking carbon flows within the building, they often rely on fixed emission factors for grid electricity, overlooking the variability in carbon intensity due to diverse energy sources. It is evident that this status quo can no longer meet the demands of the building sector, which is undergoing rapid and comprehensive decarbonization. There is a compelling need for more accurate carbon emission modeling and accounting to determine the operational strategy of BIES, taking into account the spatial and temporal dynamics of the grid's carbon intensity.

3) Handling uncertainties in multi-energy systems

Various methods have been investigated in prior research to handle uncertainties in BIES and energy hub operations. Representative methods include chance-constrained optimization, robust optimization, stochastic optimization, and lately, distributionally robust optimization. For instance, Yan et al. [32] develop a two-stage robust scheduling method for multi-energy systems, enhancing flexibility against wind energy variability. To account for the uncertainty from PV output, a distributional robust optimization (DRO) method based on Wasserstein distance is developed in [33]. A distributional robust chance-constrained (DRCC) method has been introduced in [34] to tackle uncertainties from heating demand and outdoor temperature. Xiao et al. [26] utilizes a scenario-based joint chance constraint approach for handling uncertainties in loads and renewable sources like wind and PV. These studies primarily employ stochastic or robust optimization methods. Stochastic optimization requires precise probability distributions of uncertainties, while robust optimization might lead to overly conservative outcomes, potentially diminishing solution quality. Although the data-driven set based RO method presented by [31], the chance-constraints method proposed by [30], and DRO-based IES optimization proposed in [27] address the issue of over-conservativeness, they lack statistical feasibility guarantees [35]. Research gaps: Existing methods primarily employ samples to estimate the characteristics of random variables, such as their distributions and uncertainty sets. However, there are often discrepancies between the estimated distributions and the true distributions of these random variables, leading to inaccuracies in predictions, which can result in the violation of constraints and suboptimal solutions. To address this critical challenge, the concept of statistical feasibility emerges as an effective solution to ensure that the solutions obtained from an optimization problem with chance constraints are feasible across different samples with a certain level of confidence. Statistical feasibility allows decisionmakers to derive a solution that is robust from a statistical perspective, thereby eliminating the need for assumptions about sample distribution or resampling techniques often found in the literature. To guarantee statistical feasibility, the uncertainty sets need to be properly calibrated from data, so that we can quantify the errors to be involved in the optimization process in

a probabilistic way.

C. Our Contributions

Motivated by the aforementioned research gaps, in this paper, we develop a novel carbon-aware and learning-based robust operation framework for a BIES comprising of a range of technologies, such as CCS, P2G, energy storage system, combined heat and power, absorption chiller, and electric chiller. To take carbon emissions into account accurately, we incorporate carbon trading and time-varying carbon intensity of the regional grid, along with zero-emission technologies, into the formulation of the BIES scheduling problem formulation to enable wellinformed decision-making. Then, we incorporate the uncertainties related to electricity, heating, cooling load forecast errors, PV power generation, and carbon intensity into the scheduling problem through chance-constrained optimization, which can be converted into a corresponding robust optimization problem. We propose a two-phase approach comprising shape learning and shape calibration in order to acquire an optimal uncertainty set that ensures favorable results with a statistical feasibility guarantee. The proposed approach was tested based on synthetic and real-world data. Simulation results indicate that the proposed learning-based robust optimization approach yields an average 8.2% reduction in cost and net-zero emission building, compared with performance benchmarks, while ensuring stable feasibility guarantees.

The contributions of this paper are summarized as follows:

- We develop a carbon-aware formulation for optimal BIES operation incorporating low-carbon technologies, carbon accounting, and carbon trading. Our work pioneers the integration of precise carbon emissions modeling into the BIES formulation to facilitate the zero-carbon transition of the building sector, distinguishing it from literature that concentrates primarily on minimizing operational costs.
- 2) We develop a novel two-stage learning-based uncertainty set construction algorithm that is capable of ensuring statistical feasibility. Through theoretical analysis and experimental verification, we demonstrate that the proposed algorithm guarantees that the solutions consistently adhere to satisfy the building energy and carbon consumption balance at a given confidence level.
- 3) We conduct extensive simulation studies using both synthetic and real-world datasets, showcasing the performance of the proposed approach, compared with existing performance benchmarks. The findings indicate that our approach demonstrates improved control over the violation rate and yields lower costs.

Table I provides a detailed comparison between this work and existing research efforts. It is worth noting that uncertainties persist without consideration of carbon-related factors in the building environment, and the proposed two-phase approach can work with other forms of uncertainties. However, we are incorporating carbon accounting and modeling in this manuscript to underscore the urgency and significance of transitioning towards more sustainable and environmentally friendly building practices. Through the "carbon-aware" lens, we aim to provide insights that can inform and drive effective strategies for achieving carbon reductions in the built environment.

Table I: Comparison between this study and existing approaches

Ref.	Carbon- Aware	Grid Emission Factor	Uncertainty Modeling	Distribution Assumption-Free	Violation Rate Guarantee	Statistical Feasibility Guarantee
[29]	×	×	Stochastic	×	×	X
[30]	×	X	Chance constraint	×	X	×
[31]	\checkmark	X	Robust optimization	\checkmark	\checkmark	×
[25]	\checkmark	X	Stochastic	×	X	×
[26]	\checkmark	Constant	Chance constraint	×	X	×
[27]	\checkmark	Constant	DRO	\checkmark	\checkmark	×
Our work	\checkmark	Real-time	Learning-based robust	\checkmark	\checkmark	\checkmark

The remainder of this paper is organized as follows. Section II presents the model of the carbon capture system as well as the model of BIES. Section III illustrates the solution methodology to deal with the uncertainty. The numerical studies are carried out in Section IV, and finally, the conclusions are drawn in Section V.

II. MODEL FORMULATION

This section outlines the carbon-related and other components of the BIES, crucial for achieving carbon neutrality. Components include Combined Heat and Power (CHP), Energy Storage System (ESS), Absorption Chiller (AC), Gas Boiler (GB), Electric Chiller (EC), and purchased electricity from the grid. Figure 1 illustrates the system structure and energy flow. The BIES aims to minimize costs, including energy purchases and carbon credits, through optimal operation, balancing costeffectiveness with low carbon emissions.

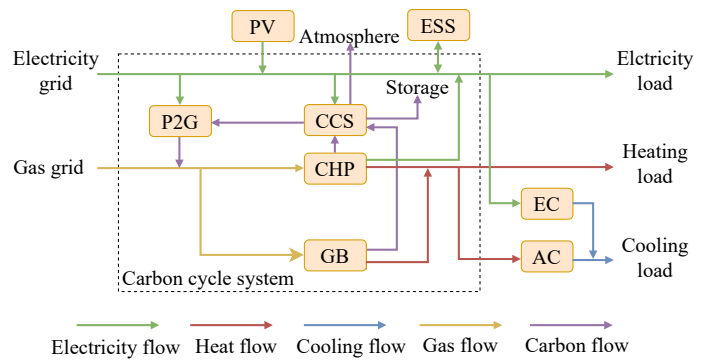


Figure 1: The brief structure of BIES and energy flow

A. Model of Carbon Cycle System (CCS)

To mitigate the carbon emissions of the system, it is essential to quantify these emissions accurately. This subsection introduces the carbon cycle system, which includes the processes of CO₂ production, capture, and utilization. Following this, we present a model for carbon accounting that provides a comprehensive framework for understanding and reducing the carbon footprint of the BIES.

Carbon production: In BIES, the CO_2 produced consists of two parts: the direct emission and the indirect emission. The direct carbon emission comes from the consumption of natural gas, and we have

$$E_{CHP,t} = \delta_a F_{CHP,t},\tag{1}$$

$$E_{GB,t} = \delta_a F_{GB,t},\tag{2}$$

where $E_{CHP,t}$ and $E_{GB,t}$ are the amount of carbon emission from CHP and GB, respectively. δ_g represents the CO₂ emission factor of natural gas. $F_{CHP,t}$ and $F_{GB,t}$ denote gas consumption of CHP and GB.

The indirect carbon emission comes from the power purchased from the main grid, and we have

$$E_{virtual} = \sum_{t=1}^{T} CI_t * P_{buy,t}, \tag{3}$$

where $P_{buy,t}$ is the purchased power from the main grid. CI_t is the carbon intensity of the main grid at time t. Calculating CI_t involves analyzing the mix of energy sources in the grid and their respective emission factors. Specifically, CI_t is determined as follows [36]:

$$CI_{t} = \frac{\sum_{k \in \mathcal{E}} ef^{k} \times M_{t}^{k}}{\sum_{k \in \mathcal{E}} M_{t}^{k}},$$
(4)

where \mathcal{E} as the set of energy sources. M_t^k represents the amount of electricity produced by source k at time t. The carbon emissions associated with electricity generation vary across different energy sources. Each source k has an associated carbon emission factor, ef^k , indicating the emissions per unit of electricity generated by this source.

Carbon intensity reflects the weighted average of carbon emissions per unit of electricity generated, considering the contribution of each energy source. Adopting dynamic carbon intensity modeling allows for more accurate environmental assessments than using a fixed emission factor, facilitating the pursuit of net-zero emissions in buildings. Real-time CI data, provided by grid operators [37] or third-party services like Electricity Map [38] and WattTime [39], enhances the precision of carbon emission calculations, supporting informed decisionmaking in energy management.

Carbon capture and utilization: The CO_2 emission captured and utilized at time t can be indicated in (5). Part of the captured CO₂ can be used as raw material for P2G process, another portion can be stored, and the rest will be emitted into the atmosphere, which can be formulated in

$$E_{CCS,t}^{cap} = \eta_{CCS} (E_{CHP,t} + E_{GB,t}), \tag{5}$$

$$F_{g,t}^{P2G} = \eta_{P2G} P_{e,t}^{P2G}, \qquad (6)$$

$$E_{CCS,t}^{P2G} = \eta_{CC} P_{e,t}^{P2G}, \qquad (7)$$

$$E_{CCS,t}^{P2G} = \eta_{CC} P_{e,t}^{P2G},\tag{7}$$

$$E_{CCS,t}^{cs} = E_{CCS,t}^{cap} - E_{CCS,t}^{P2G} - E_{CCS,t}^{atm}, \tag{8}$$

where $E^{cap}_{CSS,t}$ represents the ${\rm CO_2}$ captured via CCS at time t. $F_{g,t}^{P2G}$ is the natural gas produced via P2G process at time t. $E_{CCS,t}^{cs}$ and $E_{CCS,t}^{atm}$ represent the CO_2 is stored and emitted into the atmosphere, respectively. $P_{e,t}^{P2G}$ denotes the power consumption during the process of P2G.

In addition, the electricity consumption of CCS process at time t is indicated in

$$P_{e,t}^{CCS} = \eta_{cap} E_{CSS,t}^{cap}, \tag{9}$$

where $P_{e,t}^{CSS}$ is the power consumption during the process of

The overall direct carbon emission is determined by the difference between the emission resulting from natural gas consumption and the amount of CO_2 that is stored and utilized, which is illustrated by

$$E_{real} = \sum_{t=1}^{T} E_{CHP,t} + \sum_{t=1}^{T} E_{GB,t} - \sum_{t=1}^{T} \left(E_{CCS,t}^{P2G} + E_{CCS,t}^{cs} \right).$$
 (10)

The total carbon emission is the sum of direct real and indirect virtual carbon emissions, which is calculated by

$$E_{total} = E_{real} + E_{virtual}. (11)$$

According to the carbon emission model, there are several strategies for the system to reduce its total carbon emissions. First, the system owner can directly decrease actual carbon emissions through the implementation of CCS technologies. Second, integrating zero-emission energy sources such as PV can substitute for energy purchases, thereby reducing reliance on non-renewable sources. Third, the system can minimize indirect carbon emissions from energy purchasing by shifting load consumption to periods when carbon intensity is lower.

B. Model of Building Integrated Energy System (BIES)

The other part of the model of building integrated energy system is shown in

$$Q_t^{ESS} = Q_{t-1}^{ESS} + P_{e,t}^{ESS},$$

$$P_{min}^{ESS} \le P_{e,t}^{ESS} \le P_{max}^{ESS},$$

$$Q_{min}^{ESS} \le Q_t^{ESS} \le Q_{max}^{ESS},$$

$$(13)$$

$$P_{min}^{ESS} \le P_{e,t}^{ESS} \le P_{max}^{ESS},\tag{13}$$

$$Q_{min}^{ESS} \le Q_t^{ESS} \le Q_{max}^{ESS},\tag{14}$$

$$P_{h,t}^{CHP} = \eta_{CHP,h} F_{CHP,t},\tag{15}$$

$$P_{h,t}^{CHP} = \eta_{CHP,h} F_{CHP,t}, \qquad (15)$$

$$P_{e,t}^{CHP} = \eta_{CHP,e} F_{CHP,t}, \qquad (16)$$

$$P_{h,t}^{GB} = \eta_{GB} F_{GB,t}, \tag{17}$$

$$P_{h,t}^{AC} = \eta_{AC} P_{c,t}^{AC}, \qquad (18)$$

$$P_{c,t}^{EC} = \eta_{EC} P_{c,t}^{EC}. \qquad (19)$$

$$P_{a,t}^{EC} = \eta_{EC} P_{a,t}^{EC}. \tag{19}$$

where $Q_{ess,t}$ represents the electricity storage level of the ESS at time t. $P_{ess,t}$ is charging and discharging power of ESS at time t (positive when charging and negative when discharging). $P_{h,t}^{CHP}$ and $P_{e,t}^{CHP}$ denote heat and power generation of CHP at time t. $P_{h,t}^{CHP}$ and $P_{e,t}^{CHP}$ are heat and power generation of CHP at time t, respectively. $P_{c,t}^{AC}$ and $P_{c,t}^{EC}$ represent the refrigeration power of AC and EC, respectively. $P_{h,t}^{AC}$ denotes heat absorption power at time t. $P_{e,t}^{EC}$ is electricity consumption power of EC at time t. We utilize subscripts e, h, and c to denote the load associated with electricity, heating, and cooling, respectively. Eq. (12) - Eq. (14) limits the operation of the energy storage system. Eq. (15) - Eq. (19) are the operation models of heat production and refrigeration equipment.

C. Chance Constraints

The modeling of the power balance for electricity, heating, and cooling, as well as the carbon consumption balance, is as follows:

1) The electricity load balance constraint can be written as

$$\Pr\left(P_{e,t}^{CHP} + P_{e,t}^{PV} + P_{e,t}^{buy} \ge P_{e,t}^{load} + P_{ess,t} + P_{e,t}^{EC} + P_{e,t}^{P2G} + P_{e,t}^{CCS}\right) \ge 1 - \epsilon, \forall t \in \mathcal{T},$$
 (20)

where, $P_{e,t}^{\mathrm{buy}}$ is the purchased electricity at time t; $P_{e,t}^{PV}$ is the PV generation at time t; $P_{e,t}^{load}$ is the load of electricity at time t. Eq. (20) describes the chance-constraint of power balance.

2) The heating load balance constraint can be written as

$$\Pr\left(P_{h,t}^{CHP} + P_{h,t}^{GB} \geq P_{h,t}^{load} + P_{h,t}^{AC}\right) \geq 1 - \epsilon, \forall t \in \mathcal{T}, \quad \text{(21)}$$
 where $P_{h,t}^{load}$ is the heating load at time t . Eq. (21) describes the chance-constraint of thermal power balance.

3) The cooling load balance constraint is given by

$$\Pr\left(P_{c,t}^{EC} + P_{c,t}^{AC} \ge P_{c,t}^{load}\right) \ge 1 - \epsilon, \forall t \in \mathcal{T}, \tag{22}$$

where $P_{c.t.}^{load}$ is the cooling load at time t. Eq. (22) describes the chance-constraint of cold power balance.

4) The carbon consumption balance constraint is given by

$$\Pr\left(E_{virtual} + E_{real} - E_{buy} \le Q_{quota}\right) \ge 1 - \epsilon,\tag{23}$$

where E_{buy} is the carbon allowance purchased from the carbon market, Q_{quota} is the original carbon quota the BIES held in time period T. The building owner can sell the surplus carbon allowance to the market to make profits. Equation (23) describes the chance constraint of carbon allowance balance, which is identified as the key constraint to achieving net-zero emission.

D. Objective Function

In order to explore the economic and environmental benefits of BIES operation, the total cost includes four terms, namely energy purchased cost (EPC), carbon storage cost (CSC), and carbon trading cost (CTC).

$$Cost = C_{EPC} + C_{CSC} + C_{CTC}. (24)$$

Energy Purchased Cost (EPC): This cost incorporates the expenses for buying electricity and natural gas, represented by:

$$C_{EPC} = \sum_{t=1}^{T} p_{e,t} \cdot P_{e,t}^{buy} + \sum_{t=1}^{T} p_{gas,t} \cdot (F_{CHP,t} + F_{GB,t} - F_{g,t}^{P2G}).$$
(25)

Carbon Storage Cost (CSC): Costs associated with storing captured CO₂ are calculated as:

$$C_{CSC} = \sum_{t=1}^{T} k_{cs} \cdot E_{CCS,t}^{cs} \tag{26}$$

where k_{cs} is the cost of carbon storage.

Carbon Trading Cost (CTC): This reflects the expenses or revenues from buying or selling carbon allowances in the carbon market:

$$C_{CTC} = p_{CO_2} \cdot E_{buy}, \tag{27}$$

where p_{CO_2} is the carbon price, and E_{buy} denotes the net carbon allowances traded.

To achieve net-zero emissions, it is assumed that building owners can purchase carbon allowances to offset their emissions or sell surplus allowances to make profits. The adoption of carbon capture and storage technologies, supported by a carbon market, offers a pathway to economically viable emission reductions. This approach enables BIES operators to balance emissions with carbon trading, optimizing both economic and environmental outcomes.

The chance-constrained (CC) form of the BIES operation problem is as follows:

(CC) min
$$C_{EPC} + C_{CSC} + C_{CTC}$$

s.t. $Constraints(1) - (23)$ (28)

Eq. (20) - Eq. (23) are chance constraints. The target of the problem is to identify a feasible solution for (28) with a specified level of statistical confidence while minimizing the objective value as much as possible. In traditional CCP, knowing the distributions of the random variables is essential. With this knowledge, the non-convex CCs can be equivalently transformed into a tractable form. Detailed explanations of the transformations are provided in Appendix B.

III. METHODOLOGY

In this section, we begin by revisiting the formulation of chance-constrained programming (CCP) and present the fundamental procedural framework of our algorithm. Subsequently, we present the methodologies that have been developed in our research.

A. Proposed Framework

The common form of a CCP typically takes the following structure:

$$\min f(x); \text{ s.t. } P(g(x;\xi) \in \mathcal{A}) \ge 1 - \epsilon \tag{29}$$

where x is the decision variable, ξ is a random variable that can be observed via a finite amount of data, A is the feasible region, and ϵ is the tolerance level. Prior to delving into the specifics, the concept of statistical feasibility is introduced.

Definition 1 (Statistical Feasibility [35]). For a CC like (29), an algorithm is considered to be statistically feasible if the resulting solution, denoted as x^* , is feasible for the chance constraint with a confidence level of $1 - \delta$ for any given dataset D_{ξ} .

$$\mathbb{P}_{\mathcal{D}_{\varepsilon}} \left(\mathbb{P}_{\varepsilon} \left(g(x^*; \xi) \in \mathcal{A} \right) \ge 1 - \epsilon \right) \ge 1 - \delta \tag{30}$$

The inner constraint in (30) represents the conventional CC. Additionally, the outer constraint in (30) ensures that for all resulting solutions corresponding to different sample sets D_{ε} , the inner chance constraint can be satisfied with a probability greater than or equal to $1 - \delta$.

The original chance constraints are intractable, necessitating the use of an approximation. To tackle this challenging problem, we transform the model as outlined in (29) into a robust optimization (RO) problem. This transformation also facilitates the direct use of data [40]. RO addresses uncertainty by representing it through a deterministic set, referred to as an uncertainty set. The RO formulation ensures that the safety condition holds for any value of ξ within the uncertainty set. This helps to simplify the problem and make it more tractable. The RO form of (29) is as follows:

$$g(x;\xi) \in \mathcal{A}, \quad \forall \xi \in \mathcal{U}$$
 (31)

where $\mathcal{U} \in \Omega$ represents an uncertainty set. It is evident that for any x that is feasible for (31), if $\xi \in \mathcal{U}$ then $g(x;\xi) \in \mathcal{A}$. Therefore, by selecting an uncertainty set \mathcal{U} such that $P(\xi \in$ \mathcal{U}) $\geq 1 - \epsilon$, any feasible solution x for (31) must satisfy $P(g(x;\xi) \in \mathcal{A}) \ge P(\xi \in \mathcal{U}) \ge 1 - \epsilon.$

The motivation behind this transformation is rooted in the fact that the RO form only necessitates an uncertainty set that approximately encompasses the potential values of ξ . As a result, there is no need to make assumptions about a specific distribution for ξ . This characteristic empowers the construction of uncertainty sets learning from sample data, making the approach free from distributional assumptions.

Various advanced forecasting algorithms can be applied to predict day-ahead load and PV generation [41]. Besides, novel approaches for forecasting carbon intensity have also emerged [42]. Nonetheless, these prediction models inevitably entail some level of prediction error. These uncertainties in the prediction process can have substantial consequences on energy system planning and operation. To account for these uncertainties, expressions for uncertainties associated with loads, PV generation, and carbon intensity are as follows:

$$P_{e,t}^{PV} = \overline{P}_{e,t}^{PV} + \tilde{P}_{e,t}^{PV}, \tag{32}$$

$$P_{e,t}^{\text{load}} = \overline{P}_{e,t}^{\text{load}} + \tilde{P}_{e,t}^{\text{load}}, \tag{33}$$

$$P_{h,t}^{\text{load}} = \overline{P}_{h,t}^{\text{load}} + \tilde{P}_{h,t}^{\text{load}}, \tag{34}$$

$$P_{e,t}^{\text{load}} = \overline{P}_{e,t}^{\text{load}} + \widetilde{P}_{e,t}^{\text{load}},$$

$$P_{e,t}^{\text{load}} = \overline{P}_{h,t}^{\text{load}} + \widetilde{P}_{e,t}^{\text{load}},$$

$$P_{h,t}^{\text{load}} = \overline{P}_{h,t}^{\text{load}} + \widetilde{P}_{h,t}^{\text{load}},$$

$$P_{c,t}^{\text{load}} = \overline{P}_{c,t}^{\text{load}} + \widetilde{P}_{c,t}^{\text{load}},$$

$$(35)$$

$$I_t = \overline{I}_t + \tilde{I}_t, \tag{36}$$

where $\overline{P}_{e,t}^{PV}$, $\overline{P}_{e,t}^{load}$, $\overline{P}_{h,t}^{load}$, $\overline{P}_{c,t}^{load}$, \overline{I}_t are predicted value of dayahead PV generation, electricity load, heating load, cooling load, and carbon intensity, respectively. The random terms are denoted by $\tilde{P}_{e,t}^{PV}$, $\tilde{P}_{e,t}^{load}$, $\tilde{P}_{h,t}^{load}$, $\tilde{P}_{c,t}^{load}$, \tilde{I}_{t} and the probability distributions of random terms are not known.

Therefore, the constraints in (20) - (23) can be explicitly expressed in terms of random variables in the following form:

$$P_{e,t}^{CHP} + \overline{P}_{e,t}^{PV} + P_{e,t}^{buy} \ge \overline{P}_{e,t}^{load} + P_{e,t}^{ESS} + P_{e,t}^{EC} + P_{e,t}^{P2G} + P_{e,t}^{CCS} + \mathbf{h}^{\mathrm{T}} \boldsymbol{\xi}_{1,t}, \quad \forall \boldsymbol{\xi}_{1,t} \in \mathcal{U}_{1,t}, \forall t \in \mathcal{T},$$

$$(37)$$

$$P_{h,t}^{CHP} + P_{h,t}^{GB} \ge \overline{P}_{h,t}^{load} + P_{h,t}^{AC} + \xi_{2,t}, \quad \forall \xi_{2,t} \in \mathcal{U}_{2,t}, \forall t \in \mathcal{T},$$
(38)

$$P_{c,t}^{EC} + P_{c,t}^{AC} \ge \overline{P}_{c,t}^{load} + \xi_{3,t}, \quad \forall \xi_{3,t} \in \mathcal{U}_{3,t}, \forall t \in \mathcal{T},$$
 (39)

$$\sum_{t=1}^{T} (\overline{I}_t + \xi_{4,t}) * P_{buy,t} + E_{real} - E_{buy} \le Q_{quota}, \forall \boldsymbol{\xi_4} \in \mathcal{U}_4, \tag{40}$$

where $\boldsymbol{\xi}_{1,t} = [\tilde{P}_{e,t}^{load}, \tilde{P}_{e,t}^{PV}]^{\top}, \mathbf{h} = [1,-1]^{\top}, \boldsymbol{\xi}_{2,t} = \tilde{P}_{h,t}^{load}, \boldsymbol{\xi}_{3,t} =$ $\tilde{P}_{c,t}^{load}, \; \xi_{4,t} = \tilde{I}_t. \; \boldsymbol{\xi_4}$ is the vector form of $\xi_{4,t}, \forall t \in \mathcal{T}$. The learning-based robust optimization (LRO) problem is as follows:

(LRO) min
$$C_{EPC} + C_{CSC} + C_{CTC}$$

s.t. $Constraints(1) - (19), (37) - (40)$. (41)

B. Learning-based Robust Optimization (LRO)

Suppose the data set is $D = \{\xi_1, \dots, \xi_n\}, \xi_i \in \mathbb{R}^m$, the question then revolves around how to construct the uncertainty set. The process is considered as learning the shape of the uncertainty set by utilizing historical data. The fundamental approach aims to shrink or reduce the size of the uncertainty set $\mathcal{U} = \mathcal{U}(D)$, which covers at least $1 - \epsilon$ of the true distribution P with a confidence level of $1 - \delta$, i.e.

$$\mathbb{P}_D(P(\boldsymbol{\xi} \in \mathcal{U}(D)) \ge 1 - \epsilon) \ge 1 - \delta. \tag{42}$$

To reduce the conservativeness of the solution, two principles are employed in the construction of the uncertainty set: 1) minimizing the set size as much as possible, and 2) ensuring that $P(\xi \in \mathcal{U}(D))$ is not only greater than $1-\epsilon$, but also approaches $1 - \delta$ closely.

Following the aforementioned principles, a two-phase strategy is adopted to construct the uncertainty set \mathcal{U} . The data Dis partitioned into two groups, denoted as D_1 and D_2 , with

sizes n_1 and n_2 respectively. Let $D_1 = \{\xi_1^1,...,\xi_{n_1}^1\}$ and $D_2 = \{\xi_1^2,...,\xi_{n_2}^2\}$. The two phases can be outlined as follows:

Phase 1: Shape learning. To approximate the shape of the uncertainty set, we utilize D_1 and employ an ellipsoidal uncertainty set, which is widely used in classical robust optimization to determine the shape of samples due to its tractability [43]. It is characterized by $\{\boldsymbol{\xi} \mid (\boldsymbol{\xi} - \boldsymbol{\mu})^{\top} \boldsymbol{\Sigma}^{-1} (\boldsymbol{\xi} - \boldsymbol{\mu}) \leq s\}$, where s is a positive constant. μ and Σ are the sample mean and covariance matrix of D_1 , respectively. It enables us to determine the position of the smallest uncertainty set while providing a tractable approximation.

Phase 2: Shape calibration. To calibrate the size of the uncertainty set, we leverage D_2 and determine the appropriate value of s. The objective is to ensure that it satisfies (42) and that $\mathbb{P}_D(P(\boldsymbol{\xi} \in \mathcal{U}(D)) \approx 1 - \epsilon)$ is close to $1 - \delta$.

We first define a dimension-collapsing map $h(\cdot): \mathbb{R}^m \to \mathbb{R}$ as follows:

$$h(\boldsymbol{\xi}) = (\boldsymbol{\xi} - \boldsymbol{\mu})^{\top} \boldsymbol{\Sigma}^{-1} (\boldsymbol{\xi} - \boldsymbol{\mu}). \tag{43}$$

Using the transformation map $h(\xi)$, each sample vector ξ can be mapped to a scalar value. We apply this transformation to all $\boldsymbol{\xi}_i^2 \in D_2$ and subsequently sort the resulting values $h(\boldsymbol{\xi}_i^2)$ in ascending order to get a new list denoted as $\{\hat{s}_k, 1 \leq k \leq n_2\}$. In other words, the values in the list satisfy the inequality $\hat{s}_k \leq$ \hat{s}_{k+1} . The desired value of s corresponds to the ranking k^* of the sorted list $\{\hat{s}_k, 1 \leq k \leq n_2\}$. The index k^* is chosen such

$$k^* = \min \left\{ r : \sum_{k=0}^{r-1} C_{n_2}^k (1 - \epsilon)^k (\epsilon)^{n_2 - k} \ge 1 - \delta \right\}. \tag{44}$$

Note that here we employ an ellipsoidal uncertainty set; however, it is also applicable to use a polyhedral uncertainty set as it is typical in the classical RO approach [43]. The procedure for utilizing the polyhedron uncertainty set remains the same. The process for constructing the uncertainty set is demonstrated in Algorithm 1 in detail. We have the following statistical guarantee of the constructed uncertainty set.

Theorem 1 (Statistical guarantee for LRO). For the two datasets, $D_1 = \{\xi_1^1, ..., \xi_{n_1}^1\}$ and $D_2 = \{\xi_1^2, ..., \xi_{n_2}^2\}$. If $n_2 \ge \log \delta / \log(1 - \epsilon)$, the obtained solution \hat{x}_0 of (29) using the construct uncertainty set U satisfies the statistical feasibility guarantee.

More details of this proof can be found in [35]. Note that the sample requirement depends solely on δ and ϵ and is independent of the dimension of the random variable.

By transferring the CCs to their counterpart approximation using the classic RO form, these constraints can be subsequently converted into a tractable form once the uncertainty set has been constructed, as follows:

Theorem 2. The constraints in (37) - (40) can be equivalently transformed into the following constraints:

$$P_{e,t}^{CHP} + \overline{P}_{e,t}^{PV} + P_{e,t}^{buy} \ge \overline{P}_{e,t}^{load} + P_{e,t}^{ESS} + P_{e,t}^{EC} + P_{e,t}^{P2G} + P_{e,t}^{CCS} + \phi_{1,t}, \quad \forall t \in \mathcal{T},$$
(45)

$$P_{h,t}^{CHP} + P_{h,t}^{GB} \ge \overline{P}_{h,t}^{load} + P_{h,t}^{AC} + \phi_{2,t}, \quad \forall t \in \mathcal{T},$$
 (46)

$$P_{c,t}^{EC} + P_{c,t}^{AC} \ge \overline{P}_{c,t}^{load} + \phi_{3,t}, \quad \forall t \in \mathcal{T},$$

$$(47)$$

$$\sum_{t=1}^{T} \overline{I}_t * P_{buy,t} + E_{real} - E_{buy} + \phi_4 \le Q_{quota}, \tag{48}$$

where $\phi_{1,t}, \phi_{2,t}, \phi_{3,t}$, and ϕ_4 satisfy

$$\phi_{1,t} = \mathbf{h}^{\top} \boldsymbol{\mu}_{1,t} + \sqrt{s_{1,t}} \left\| \boldsymbol{\Sigma}_{1,t}^{1/2} \mathbf{h} \right\|_{2}, \tag{49}$$

$$\phi_{2,t} = \mu_{2,t} + \sqrt{s_{2,t}} \left\| \Sigma_{2,t}^{1/2} \right\|_2, \tag{50}$$

$$\phi_{3,t} = \mu_{3,t} + \sqrt{s_{3,t}} \left\| \Sigma_{3,t}^{1/2} \right\|_2, \tag{51}$$

$$\phi_4 = \mathbf{P}_{buy}^{\top} \boldsymbol{\mu}_{1,t} + \sqrt{s_{4,t}} \left\| \boldsymbol{\Sigma}_4^{1/2} \mathbf{P}_{buy} \right\|_2.$$
 (52)

 P_{buy} denotes the vector form of $P_{buy,t}$. The details of the proof are provided in Appendix B. Note that then the problem is a second-order cone program (SOCP) problem which is convex and can be solved by standard solvers such as CPLEX and Gurobi. By utilizing the shape parameters of the constructed uncertainty set, we can then reformulate the new problem (41) as an equivalent deterministic problem that is more tractable.

Algorithm 1 Learning-based Uncertainty Set Construction

Input:
$$\overline{P}_{e,t}^{PV}, P_{e,t}^{PV}, \overline{P}_{e,t}^{load}, P_{e,t}^{load}, \overline{P}_{h,t}^{load}, P_{h,t}^{load}, \overline{P}_{c,t}^{load}, P_{c,t}^{load}$$

Output: The uncertainty set $\mathcal{U}_{1,t}(\xi_{1,t})$, $\mathcal{U}_{2,t}(\xi_{2,t})$, $\mathcal{U}_{3,t}(\xi_{3,t})$, $\mathcal{U}_4(\boldsymbol{\xi}_4)$

- 1: Compute the set of electricity load, heating load, cooling load, and carbon intensity prediction errors $D_{1,t}, D_{2,t}, D_{3,t}, D_4$ according to Eq. (32) - (35), respectively;
- 2: Divide $D_{1,t}$ into two groups $D_{1,t}^1$ and $D_{1,t}^2$, with sizes n_1 and n_2 ,
- 3: Estimate the sample mean $\mu_{1,t}$ and covariance matrix $\Sigma_{1,t}$ on $D_{1,t}^1$;
- 4: Construct the dimension-collapsing map $h(\cdot)$ according to (43) and
- calculate the transformed value $t(\boldsymbol{\xi}_{1,t})$ for all $\boldsymbol{\xi}_{1,t} \in D^2_{1,t}$; Sort all sort the resulting values $t(\boldsymbol{\xi}_{1,t})$ in ascending order to obtain the new list $\{\hat{s}_k, 1 \leq k \leq n_2\}$ and compute the index k^* using Eq. (44) for $U_{1,t}$;
- 6: Set $s_{1,t}$ according to the obtained value corresponding to index k^* and get the uncertainty set for sample $D_{1,t}$ $\mathcal{U}_{1,t}(\boldsymbol{\xi}_{1,t}) =$ $\{ \boldsymbol{\xi}_{1,t} | t(\boldsymbol{\xi}_{1,t}) \leq s_{1,t} \};$
- 7: Construct the uncertainty set for $\mathcal{U}_{2,t}(\xi_{2,t}), \mathcal{U}_{3,t}(\xi_{3,t})$, and $\mathcal{U}_4(\boldsymbol{\xi}_4)$ following the same process outlined in Steps 2 - 6.

C. Reconstructed Learning-based Robust **Optimization** (ReLRO)

Despite constructing the uncertainty set in subsection III-B, the resulting solutions to the problem can still exhibit conservativeness. This is because the construction of \mathcal{U} is independent of the obtained solution \hat{x} . Although $P(g(\hat{x}; \boldsymbol{\xi}) \in \mathcal{A}) \geq P(\boldsymbol{\xi} \in \mathcal{U})$, the actual confidence level of $\mathbb{P}_D(P(\boldsymbol{\xi} \in \mathcal{U}(D)) \geq 1 - \epsilon)$ remains excessively conservative. In this section, our objective is to further mitigate the conservation present in the solutions.

The key idea in this approach is to incorporate the knowledge relevant to the optimization problem when constructing the uncertainty set. We can still use a two-phase approach to solve this problem. In Phase 1, the method described in Section III B is utilized to identify the uncertainty set, and a solution \hat{x} for (29) is obtained. The resulting uncertainty set takes the form $\{\xi|g(\hat{x_0};\boldsymbol{\xi})\in\mathcal{A}\}$. In Phase 2, the size of the reshaped set is adjusted, resulting in $\{\xi | g(\hat{x_0}; \boldsymbol{\xi}) \in \hat{\mathcal{A}}\}\$, where $\hat{\mathcal{A}}$ represents the size-tuned uncertainty set.

In particular, we concentrate on analyzing the carbon balance condition (40), while similar analysis can be conducted for the other constraints. For an uncertainty set \mathcal{U}_4 and its corresponding solution $\{P_{buy,t}, E_{buy}, E_{real}\}$, the following condition is satisfied:

$$\mathbb{P}_{\xi}\left(oldsymbol{\xi}\in\mathcal{U}_{4}
ight)\leq$$

$$\mathbb{P}_{\xi} \left(\sum_{t=1}^{T} (\overline{I}_t + \xi_{4,t}) * \hat{P}_{buy,t} + \hat{E}_{real} - \hat{E}_{buy} \le Q_{quota} \right) \tag{53}$$

Therefore, the following uncertainty set can be considered as a viable solution:

$$\mathcal{U}_{4} = \left\{ \boldsymbol{\xi} | \sum_{t=1}^{T} (\overline{I}_{t} + \xi_{4,t}) * \hat{P}_{buy,t} + \hat{E}_{real} - \hat{E}_{buy} \leq Q_{quota} + \alpha \right\}$$
(54)

Once again, we partition the dataset of carbon intensity forecast error D_4 into D_4^1 and D_4^2 , with respective sizes n_1 and n_2 . The dataset D_4^1 is used to estimate $\{\hat{P}_{buy,t}, \hat{E}_{buy}, \hat{E}_{real}\}$, while D_4^2 is used to estimate α . In this section, we present the construction process for \mathcal{U}_4' , while noting that the construction of $\mathcal{U}_{1,t}', \mathcal{U}_{2,t}'$, and $\mathcal{U}_{3,t}'$ can be accomplished using the same procedure. The two-phase approach is outlined as follows:

Phase 1: Shape learning. Run algorithm 1 based on D_4^1 to get the initial solution $\{\tilde{P}_{buy,t}, \tilde{E}_{buy}, \tilde{E}_{real}\}$.

Phase 2: Shape calibration. The calibration for α follows a similar approach as that in LRO. To achieve this, we introduce a customized dimension-collapsing map $h_{Recon}(\cdot): \mathbb{R}^m \to \mathbb{R}$, which is designed as follows:

$$h_{Recon}(\xi) = \sum_{t=1}^{T} (\bar{I}_t + \xi_{4,t}) * \hat{P}_{buy,t} + \hat{E}_{real} - \hat{E}_{buy} - Q_{quota}$$
(55)

Following a similar approach as in LRO, we employ the transformation $h_{Recon}(\xi)$ to map each sample vector ξ_i in D_1 to a scalar value, which is then sorted in ascending order. The desired value corresponds to the ranking k^* , where k^* is computed using (44).

The process for constructing the uncertainty set is detailed in Algorithm 2. And the performance improvement guarantee indicates that by reconstructing the uncertainty set, despite the slightly increased computational cost, we can enhance the performance of the original LRO.

Algorithm 2 Uncertainty Set Reconstruction

Input:
$$\overline{P}_{e,t}^{PV}, P_{e,t}^{PV}, \overline{P}_{e,t}^{load}, P_{e,t}^{load}, \overline{P}_{h,t}^{load}, P_{h,t}^{load}, \overline{P}_{c,t}^{load}, P_{c,t}^{load}$$
 $\overline{I}_t, I_t, \delta, \epsilon$

Output: The reconstructed uncertainty set $\mathcal{U}_{1,t}(\boldsymbol{\xi}_{1,t})'$, $\mathcal{U}_{2,t}(\boldsymbol{\xi}_{2,t})'$, $\mathcal{U}_{3,t}(\boldsymbol{\xi}_{3,t})'$, $\mathcal{U}_{4}(\boldsymbol{\xi}_{4})'$

- 1: Compute the set of electricity load, heating load, cooling load, and carbon intensity prediction errors $D_{1,t}, D_{2,t}, D_{3,t}, D_4$ according to (32) (35), respectively;
- 2: Divide D_4 into two groups D_4^1 and D_4^2 , with sizes n_1 and n_2 , respectively;
- 3: Call Algorithm 1 to compute the approximate solutions $\{\hat{P}_{buy,t},\hat{E}_{buy},\hat{E}_{real}\}$ with respect to D_4^1
- 4: Construct the dimension-collapsing map $h_{Recon}(\cdot)$ according to Eq.(55) and calculate the transformed value $h_{Recon}(\boldsymbol{\xi}_4)$ for all $\boldsymbol{\xi}_4 \in D_4^2$:
- Sort all sort the resulting values h_{Recon}(ξ₄) in ascending order to obtain the new list {ŝ_k, 1 ≤ k ≤ n₂} and compute the index k* using (44) for U'₄;
- 6: Set α according to the obtained value corresponding to index k^* and get the uncertainty set for sample D_4 such that $\mathcal{U}_4(\boldsymbol{\xi}_4)' = \{\boldsymbol{\xi}_4 | t(\boldsymbol{\xi}_4) \leq \alpha\}$;
- 7: Construct the uncertainty set for $U_{1,t}(\xi_{1,t})$, $U_{2,t}(\xi_{2,t})$, and $U_{3,t}(\xi_{3,t})$ following the same process outlined in Steps 2 6.

Table II: Relevant parameters for BIES

Parameters	Values	Parameters	Values
k_{cs} (\$/kg) η_{CC}	0.08 1.06	$\eta_{CHP,e} \ \eta_{CHP,h}$	0.35 0.45
$\delta_{e,a} \ \delta_{g,a}$	0.3 1.08	$\eta_{GB,h} \ \eta_{AC}$	0.95 1.2
$\eta_{P2G} \ Q_{ess,max}$ (kWh)	0.55 300	$\eta_{EC} \ Q_{quota}$ (kg)	4 8000

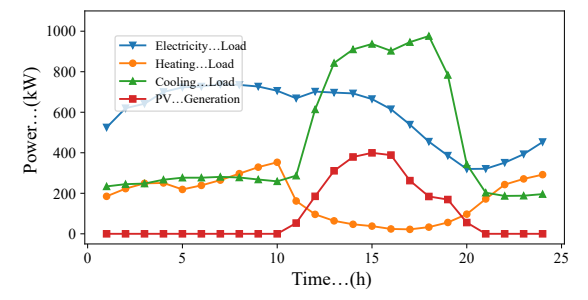


Figure 2: Load profile of the BIES for a day

IV. NUMERICAL STUDIES

A. Data Description and Experimental Settings

In this section, we conduct comprehensive numerical studies to demonstrate the accuracy of our carbon model, validate the performance of our proposed learning-based robust algorithms, and analyze the sensitivity of key parameters. The parameters required for the components in the BIES are listed in Table 1, which are set based on the research papers [2] and [27]. The time horizon of the delivery day is divided into 24 hours. For each setting, we repeat the experiments 300 times. All of the following simulations were implemented using Matlab R2022b software on a desktop computer with an Intel ® i9 2.4GHz CPU and 32GB RAM. The optimization problem is solved using CPLEX 12.8.

The electricity price data is sourced from [44], ensuring that our simulations are based on realistic market conditions. The building load and PV generation data are modified based on the End-Use Load Profiles for the U.S. Building Stock [45], a widely recognized dataset in building energy research. In Figure 2, the purple line represents the PV generation, while the blue, red, and yellow lines depict the electricity, heating, and cooling load profiles for a single day, respectively. The historical source mix data is obtained from California Independent System Operator [37]. Figure 3 illustrates the carbon intensity profile during a single day, reflecting the variations in carbon emissions throughout the day.

By utilizing realistic data and settings, we aim to ensure the validity and practicality of our simulations, enabling meaningful insights into the performance and sensitivity of the proposed learning-based robust algorithms.

B. Benchmarks and Evaluation Metrics

Our proposed methods as outlined in Sections III and IV are designated as LRO and ReLRO. In order to evaluate the performance of our approaches, we compare them with other common methods in decision-making under uncertainty:

1) Chance-constrained Optimization (CC): The conventional chance-constrained methods [46], as commonly employed in various fields, typically operate under the assumption of a

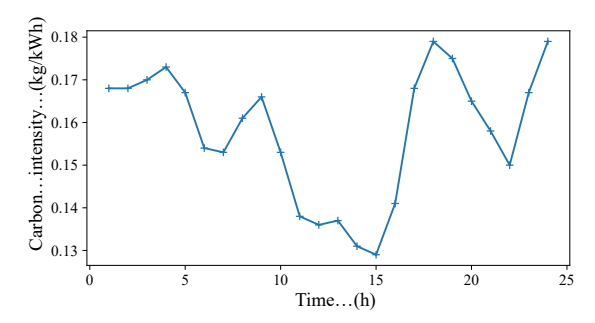


Figure 3: Carbon intensity for a day

specific distribution family for the random variable. In this study, we make the supposition that the prediction error conforms to a Gaussian distribution.

- 2) Scenario Generation (SG): The scenario generation method, introduced in [47], replaces the chance constraint with a set of sampled constraints. It is important to note that SG relies on an adequate number of samples, and the running time of SG increases linearly with the size of the sample.
- 3) Distributionally Robust Chance-Constrained (DRCC): Our proposed methods are compared with distributionally robust chance-constrained methods outlined in [48]. In this method, the probability distribution of the data is not fully required, but rather it is known to belong to a predetermined class of distributions.
- 4) The Optimal Baseline (OPT): The optimal baseline method considered in this study is deterministic optimization with perfect predictions, denoted as OPT. In this approach, all predictions and input parameters are assumed to be completely accurate, allowing for an optimal solution to be determined without considering any uncertainty or variability.

For synthetic scenarios, we adopt the definition proposed in [35]. We denote $\hat{\epsilon}$ as the estimated expected violation probability of the obtained solution. More specifically, $\hat{\epsilon}$ is calculated as $\hat{E}_D\left[P_{\mathrm{vio}}\right]$, where $\hat{E}_D\left[\cdot\right]$ represents the empirical expectation. Here, P_{vio} refers to the probability $P(g(\hat{x}(D);\xi)\notin\mathcal{A})$. Additionally, the statistic violation rate $\hat{\delta}$ is $\hat{P}_D\left(P_{\mathrm{vio}}>\hat{\epsilon}\right)$. For approaches not reliant on data, the chance constraint is always fulfilled, yielding $\hat{\delta}=0$. The experiment is conducted on 300 different sample sets. We generate the samples randomly from a multivariate Gaussian distribution with a positive-definite covariance matrix, which is widely adopted to model the load prediction error in literature [49] [50]. Note that in the realworld data experiments, we do not assume the distribution and use the real prediction error. Since there are many chance constraints, we only focus on the carbon balance violation rate.

C. Performance Analysis for Synthetic Data

1) Sensitivity Analysis for Sample Size: To assess the influence of sample size, we conduct 300 trials for each of the five different approaches, varying the sample sizes. Figures 4 and 5 illustrate how the total cost and violation rate of different approaches change with the sample size. It is noted that the performance trend varies significantly among the different methods analyzed. Specifically, the total cost and violation rate of the CC and DRCC approaches do not change substantially with increasing sample size. This can be attributed to the fact that these methods primarily rely on parametric estimation of the sample distribution. Table III indicates that for the CC approach,

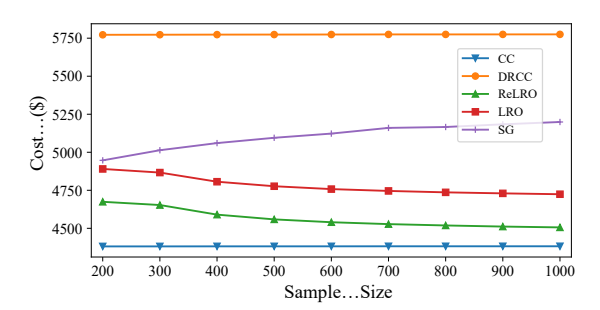


Figure 4: Cost under different sample size

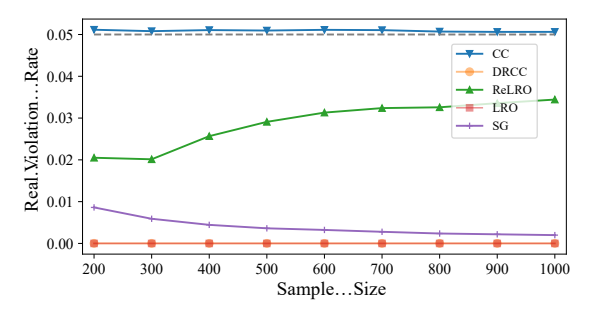


Figure 5: Real violation rate under different sample size

the observed violation rate exceeds the prescribed requirement, with a statistic violation rate of approximately 0.5. For the SG method, the total cost increases with the rising sample size, while the violation rate decreases.

For our proposed ReLRO approach, Table III demonstrates that the statistic violation rate is approximately 0.05. With an increasing sample size, our ReLRO method effectively leverages the flexibility reserve provided by the chance constraints, providing a less conservative solution that satisfies the prescribed conditions while also exhibiting an increasing violation rate.

Table IV presents the running time of the various approaches analyzed. For the SG approach, it is evident that the running time increases proportionally with larger sample sizes, which can make the computation time quite extensive for large sample sizes. However, the running time of the other algorithms shows minimal fluctuations with changing sample sizes, suggesting that the sample size does not noticeably impact the computation time for these methods. The running time of the ReLRO approach is slightly higher than the LRO because ReLRO can be regarded as solving the LRO twice. Despite the marginally increased runtime, ReLRO improves the performance of the solution, rendering the associated computational cost worthwhile.

2) Sensitivity Analysis for Violation Level Control: Figures 6 and 7 depict the performance of various approaches under different stability requirements $1-\epsilon$. First, we observe that for CC, the curve lies slightly above the stability requirement, which indicates that the CC approach does not guarantee compliance with the chance constraints in all cases. In contrast, the SG approach consistently generates feasible solutions while offering improved economic performance as $1-\epsilon$ decreases. But the total cost is the highest when ϵ is greater than 0.1, which means that it is more conservative than other methods. However, the violation rate curve of our proposed ReLRO method consistently remains lower than the allowed risk. These findings emphasize the strength of our proposed ReLRO approach in terms of effectively leveraging flexibility reserves and providing solutions that are both cost-efficient and compliant with the given chance

Table III: Statistic violation rate under different sample size

Sample	CC	SG	DRCC	LRO	ReLRO
200	0.51	0	0	0	0.046667
300	0.446667	0	0	0	0.023333
400	0.503333	0	0	0	0.03
500	0.486667	0	0	0	0.033333
600	0.486667	0	0	0	0.056667
700	0.49	0	0	0	0.046667
800	0.48	0	0	0	0.053333
900	0.493333	0	0	0	0.046667
1000	0.486667	0	0	0	0.063333

Table IV: Runing time under different sample size (s)

Sample	CC	SG	DRCC	LRO	ReLRO
200	1.136196	11.97335	1.173524	0.570546	2.705187
300	1.150944	13.76358	1.177605	0.588166	1.939536
400	1.142088	20.03871	1.433913	0.590878	1.768694
500	1.37538	26.45544	1.315433	0.584426	2.168233
600	1.15595	35.35467	1.164011	0.704867	2.232307
700	1.168317	40.99384	1.394985	0.58639	2.330702
800	1.678593	51.29287	1.158964	0.642918	1.993813
900	1.298453	57.48193	1.646797	0.69297	1.682798
1000	1.165364	67.98769	1.404033	0.643389	2.035873

constraints, even under more stringent stability requirements.

D. Performance Analysis for Real Data

In this subsection, we evaluate the performance of our algorithm using real prediction data. To accomplish this, we construct neural networks dedicated to forecasting the day-ahead load, PV generation, and carbon intensity. In order to make predictions, we utilize the data from the previous day. The training set is employed for both training the prediction model and constructing the uncertainty set, while the test set is utilized to calibrate the uncertainty set and evaluate the performance. And the result in this subsection is the average value in of 120 test days.

1) The performance of in real data. In our evaluation, we quantify the average savings in the total cost by comparing it to the optimal benchmark OPT. This comparison is expressed as a percentage, donated as the regret percentage (REP). The REP represents the gap between the achieved cost and the optimal cost, thereby indicating the relative cost-effectiveness of the evaluated methods.

Figure 8 illustrates the average REP and violation rate. Notably, the ReLRO method achieves the lowest REP (12.67%), outperforming other methods by at least 8.2% while keeping the violation rate beneath the predetermined threshold of 0.2. The findings from the real data experiment align with those observed in the synthetic dataset. The CC method exhibits a higher average REP (20.81%) than ReLRO and its violation rate surpasses the predefined threshold. It arises from the CC method's assumption of a Gaussian distribution in the data, which proves inadequate when the prediction errors deviate from this distribution. Despite the SG method achieving a zero violation rate, its REP is the highest, indicating an overconservative approach in the real dataset.

2) The impacts of different carbon emission accounting models: In this part, we evaluate three distinct scenarios, each employing a different model for carbon emission accounting. These models are designated as M1, M2, and M3 for ease of reference.

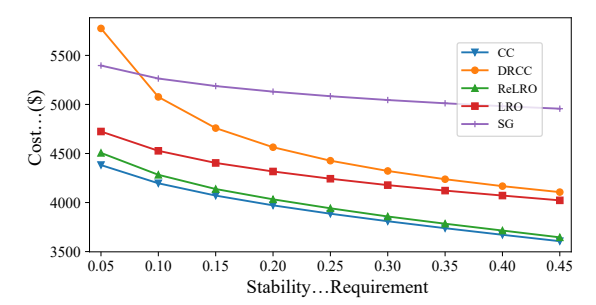


Figure 6: Cost of different stability requirement

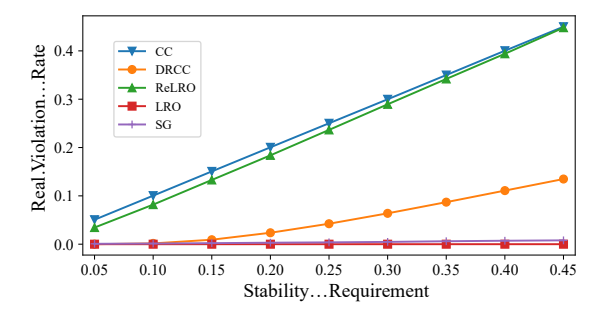


Figure 7: Real violation rate under different stability requirement

- M1: The emission factor is set at zero, indicating that we do not consider the carbon emission by the electricity purchased from the grid. It is widely employed in the literature [31] [51].
- M2: It is assumed that all electricity generation is coalbased, which is the same as the assumptions made in [27] and [26]. The emission intensity is set to 0.993 kg/kWh based on the report of [38].
- M3: This is the proposed real-time carbon intensity model.
 It calculates grid emissions on an hourly basis, offering a more accurate method for carbon accounting.

Figure 9 and 10 represent the average carbon emissions and costs under different carbon accounting models, respectively. With the grid emission factor at zero, as in M1, the model overlooks grid emissions, leading to a lower estimation of overall carbon emissions. This underestimation is critical as grid-sourced electricity is a major contributor to total emissions. In the M2 scenario, where the emission factor is 0.993 kg/kWh, assuming all electricity is coal-fired, there is a tendency to overestimate emissions. This overestimation occurs because the actual grid mix includes renewable energy sources. In contrast, our M3 model, which integrates real-time carbon intensity, provides a more nuanced and accurate depiction of the carbon system within BIES. This approach enhances the effectiveness of decision-making processes by offering a more realistic view of carbon emissions. Additionally, we believe that a key advantage of an accurate carbon accounting model is its potential to enable buildings to lower emissions through strategic load shifting, such as adjusting cooling or heating schedules and optimizing ESS operations. If the emission factor remains constant, buildings cannot achieve emission reductions by utilizing electricity during periods of low carbon intensity.

Besides, Figures 9 and 10 demonstrate that our methods effectively handle uncertainty and consistently outperform other methods under different carbon accounting models. In models M1 and M2, carbon emissions are accounted for using a fixed

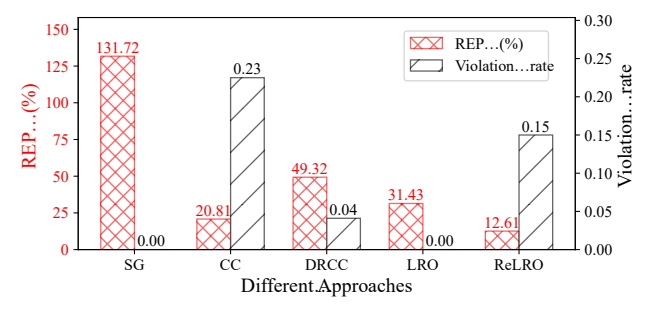


Figure 8: REP under different approaches ($\delta = 0.2$, $\xi = 0.2$)

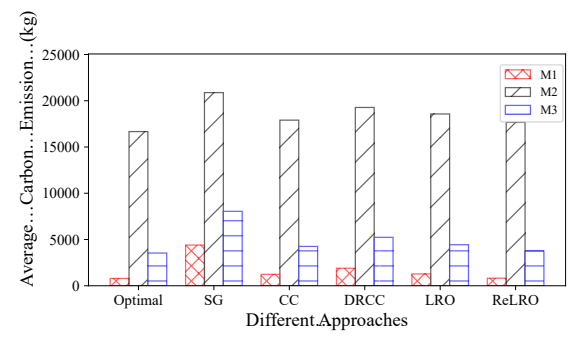


Figure 9: Average carbon emission under different grid emission accounting model

constant, thereby eliminating uncertainties related to carbon intensity. Across the various models, the SG method and the DRCC method tend to yield more conservative results, a finding that corroborates previous observations. In M3, our method stands out for its superior performance in handling different carbon accounting scenarios to reduce carbon emissions by at least 13.8%. But in M1, our model only achieves 1.4%. Because the total carbon emission is overestimated thus diminishing the impacts of uncertainties.

- 3) The impacts of different carbon prices: Figure 11 depicts the impact of different carbon pricing on emissions reduction through various methods. With perfect prediction, comparing a carbon price increase from \$0.05/kg to \$0.10/kg results in a 22.36% decrease in average emissions. Yet, elevating the price to \$0.20/kg only reduces emissions by 1.90%, indicating diminishing returns at higher price levels due to limits in the system's adaptability. These findings reveal a significant relationship between increasing carbon prices and decreased carbon emissions, emphasizing the effectiveness of appropriate carbon pricing strategies in reducing carbon footprint.
- 4) The effectiveness of CCS: In this subsection, we assess the effectiveness of CSS technology. It should be noted that implementing CCS technology as a standalone solution for emission reduction may not be economically feasible. The integration of a carbon market could provide an incentive for companies to adopt CCS technology by converting emission reductions into economic advantages. Figure 12 illustrates the direct emissions, indirect emissions, and carbon captured by the CSS under varying carbon price scenarios. In the optimal scenario where the carbon price is \$0.10/kg, the CCS system reduces total carbon emissions by 29.35%. However, at a lower carbon price of \$0.05/kg, the reduction in carbon emissions drops to 9.01%. This underscores that the carbon price is a crucial determinant of CCS utilization.

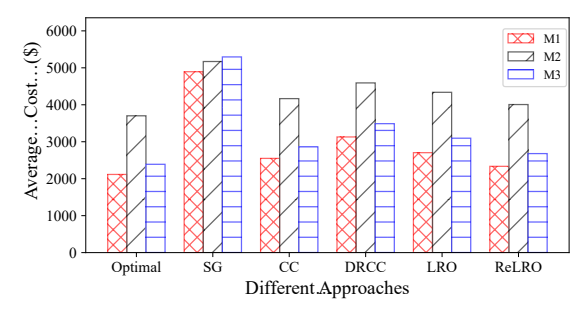


Figure 10: Average cost under different grid emission accounting model

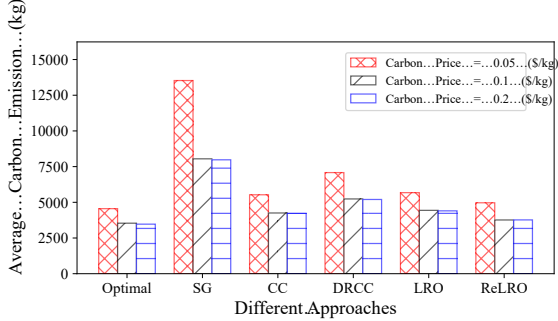


Figure 11: Carbon emission under different carbon price

V. CONCLUSION

Decarbonizing the building sector is crucial for achieving climate neutrality. In this paper, we have devised a carbonconscious optimization strategy to enable the efficient operation of diverse components and processes within building integrated energy systems, such as combined heat and power, energy storage, carbon capture, and the import of electricity from the primary grid. The proposed model aims to minimize the overall energy expenses while simultaneously curbing carbon emissions toward net-zero. Furthermore, to address the uncertainties inherent in the BIES, we have developed a robust learning-based optimization framework that provides statistical feasibility guarantees. The approach effectively handles the uncertainties and ensures reliable and robust operation by designing the appropriate uncertainty set. The proposed approach has been validated through numerical studies conducted using both synthetic and real data. Using synthetic data, our approach demonstrates improved control over the violation rate and leads to lower costs. Meanwhile, when applied to real-world data, the proposed approach achieves a significant reduction in regret percentage of over 8% for BIES control, compared to other methods in the literature. The algorithms in this work use an ellipsoidal uncertainty set to learn the shape of uncertainties. Future research could investigate the application of deep learning techniques to learning a more complex shape of the uncertainty set, thereby enhancing the precision.

VI. APPENDIX

A. Details about the Prediction Models

In the numerical studies, we construct distinct neural networks to predict day-ahead load, photovoltaic power generation, and carbon intensity, respectively. We employ the widely used multi-layer perceptron (MLP) [52] models for predictions. Considering the example of electricity load prediction, the model utilizes demand data from the preceding 24 hours as input to forecast the subsequent day's demand. Additional parameters

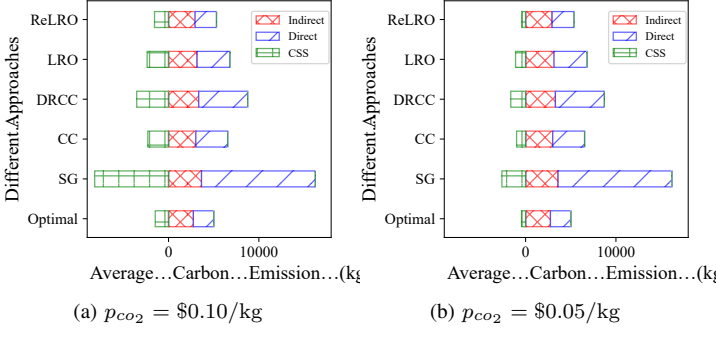


Figure 12: Direct emission, indirect emission and carbon reduction by CSS under different carbon prices

Table V: Relevant parameters for prediction models

Parameters	Values
Hidden layer size	256
# of hidden layers	2
Batch size	16
Optimizer	Adam
Activation	ReLU
Learning rate	0.001

are detailed in Table V. We partition the dataset into two segments: 55% for training the prediction model and constructing uncertainty sets, and 45% for testing and calibrating the uncertainty set.

B. Reformulation for Traditional CCs

For the traditional CCP, it is necessary to know the distribution of the random variable. Here, we use constraint (20) as an example. If $\xi_{1,t}$ follows Gaussian distribution, the intractable CC can be transformed into a deterministic convex problem, as outlined in [46].

Consider $\xi_{1,t} \sim N\left(\mu_{1,t}, \Sigma_{1,t}\right)$, and Φ^{-1} denotes the inverse cumulative distribution function of the standard normal distribution. It follows that

Prob
$$(\mathbf{h}^{\top} \boldsymbol{\xi}_{1,t} \leq b) = \Phi\left(\frac{b - \mathbf{h}^{\top} \boldsymbol{\mu}_{1,t}}{\sqrt{\mathbf{h}^{\top} \boldsymbol{\Sigma}_{1,t} \mathbf{h}}}\right),$$
 (56)

where

$$b = \overline{P}_{e,t}^{load} + P_{e,t}^{ESS} + P_{e,t}^{EC} + P_{e,t}^{P2G} - (P_{e,t}^{CHP} + \overline{P}_{e,t}^{PV} + P_{e,t}^{buy})$$
(57)

Thus,

Prob
$$(\mathbf{h}^{\top} \boldsymbol{\xi}_{1,t} \le b) \ge 1 - \epsilon \iff$$

 $b - \mathbf{h}^{\top} \boldsymbol{\mu}_{1,t} \ge \Phi^{-1} (1 - \epsilon) \left\| \boldsymbol{\Sigma}_{1,t}^{1/2} \mathbf{h} \right\|_{2}$ (58)

Therefore, the equivalent constraints are

$$P_{e,t}^{CHP} + \overline{P}_{e,t}^{PV} + P_{e,t}^{buy} \ge \overline{P}_{e,t}^{load} + P_{e,t}^{ESS} + P_{e,t}^{EC} + P_{e,t}^{P2G} + P_{e,t}^{CCS} + \mathbf{h}^{\top} \boldsymbol{\mu}_{1,t} + \Phi^{-1} (1 - \epsilon) \left\| \boldsymbol{\Sigma}_{1,t}^{1/2} \mathbf{h} \right\|_{2}$$
(59)

By following this procedure, deterministic formulations for the remaining chance constraints can be derived. Note that when the random variable has an additive relationship with the decision variables, it results in linear constraints. When the random variable has a multiplicative relationship with the decision variables, it results in second-order cone constraints. Both types of constraints can be solved efficiently using standard solvers.

C. Proof for Theorem 2

By utilizing the shape parameters of the constructed uncertainty set, the problem (41) can be reformulated as a more tractable equivalent one. As an example, consider constraint (37) and the constructed ellipsoidal uncertainty set as follows:

$$\mathcal{U}_{1,t} = \left\{ \boldsymbol{\xi}_{1,t} : \left(\boldsymbol{\xi}_{1,t} - \boldsymbol{\mu}_{1,t} \right)^{\top} \boldsymbol{\Sigma}_{1,t}^{-1} \left(\boldsymbol{\omega}_{1,t} - \boldsymbol{\mu}_{1,t} \right) \le s_{1,t} \right\},$$
(60)

Average...Carbon...Emission...(kg) where $\mu_{1,t}$, $\Sigma_{1,t}$ represent the sample mean and covariance matrix of $\xi_{1,t}$, respectively, and $s_{1,t}$ is a positive scalar value determined using Algorithm 1. The RO form is:

$$P_{e,t}^{CHP} + \overline{P}_{e,t}^{PV} + P_{e,t}^{buy} \ge \overline{P}_{e,t}^{load} + P_{e,t}^{ESS} + P_{e,t}^{EC} + P_{e,t}^{P2G} + P_{e,t}^{CCS} + \mathbf{h}^{\top} \boldsymbol{\xi}_{1,t}, \quad \forall \boldsymbol{\xi}_{1,t} \in \mathcal{U}_{1,t}, \forall t \in \mathcal{T}.$$
(61)

Note that the random variable has an additive relationship with the decision variables. Thus, the following substitution can be made:

$$\begin{split} P_{e,t}^{CHP} + \overline{P}_{e,t}^{PV} + P_{e,t}^{buy} &\geq \overline{P}_{e,t}^{load} + P_{e,t}^{ESS} + P_{e,t}^{EC} + P_{e,t}^{P2G} \\ + P_{e,t}^{CCS} + \phi_{1,t}, \quad \forall t \in \mathcal{T} \end{split} \tag{62}$$

where $\phi_{1,t}$ satisfies:

$$\phi_{1,t} = \max \quad \mathbf{h}^{\top} \boldsymbol{\xi}_{1,t}$$
s.t. $(\boldsymbol{\xi}_{1,t} - \boldsymbol{\mu}_{1,t})^{\top} \boldsymbol{\Sigma}_{1,t}^{-1} (\boldsymbol{\xi}_{1,t} - \boldsymbol{\mu}_{1,t}) \le s_{1,t}$ (63)

Slater's condition ensures that strong duality holds, thus we have:

$$\phi_{1,t} = \max_{\lambda} \min_{\boldsymbol{\xi}_{1,t}} -\mathbf{h}^{\top} \boldsymbol{\xi}_{1,t}$$
$$+ \lambda \left(\left(\boldsymbol{\xi}_{1,t} - \boldsymbol{\mu}_{1,t} \right)^{\top} \boldsymbol{\Sigma}_{1,t}^{-1} (\boldsymbol{\xi}_{1,t} - \boldsymbol{\mu}_{1,t}) - s_{1,t} \right)$$
s.t. $\lambda \geq 0$ (64)

Due to the positive definiteness of the covariance matrix $\Sigma_{1,t}$, the quadratic programming problem can be solved directly. Consequently, we can also derive explicit representations for $\phi_{1,t}$, $\phi_{2,t}$, $\phi_{3,t}$, and ϕ_4 , respectively.

REFERENCES

- [1] U.S. Environmental Protection Agency. Climate Change Indicators: Greenhouse Gases. [Online]. Available: https://www.epa.gov/climate-indicators/greenhouse-gases
- [2] P. Duan, B. Zhao, X. Zhang, and M. Fen, "A day-ahead optimal operation strategy for integrated energy systems in multi-public buildings based on cooperative game," *Energy*, vol. 275, no. 14, p. 127395, July 2023.
 [3] C. Zhang, Y. Xie, H. Zhang, Y. Gu, and X. Zhang, "Optimal design
- [3] C. Zhang, Y. Xie, H. Zhang, Y. Gu, and X. Zhang, "Optimal design and performance assessment for a solar powered electricity, heating and hydrogen integrated energy system," *Energy*, vol. 262, no. 1, p. 125453, January 2023.
- [4] H. A. Toosi, M. Lavagna, F. Leonforte, C. Del Pero, and N. Aste, "Building decarbonization: Assessing the potential of building-integrated photovoltaics and thermal energy storage systems," *Energy Reports*, vol. 8, no. 16, pp. 574–581, December 2022.
- [5] G. Ruan, H. Zhong, G. Zhang, Y. He, X. Wang, and T. Pu, "Review of learning-assisted power system optimization," *CSEE Journal of Power and Energy Systems*, vol. 7, no. 2, pp. 221–231, 2020.
- [6] S. Sharma, A. Verma, Y. Xu, and B. K. Panigrahi, "Robustly coordinated bi-level energy management of a multi-energy building under multiple uncertainties," *IEEE Transactions on Sustainable Energy*, vol. 12, no. 1, pp. 3–13, 2019.
- [7] C. Zhang, Y. Xu, Z. Li, and Z. Y. Dong, "Robustly coordinated operation of a multi-energy microgrid with flexible electric and thermal loads," *IEEE Transactions on Smart Grid*, vol. 10, no. 3, pp. 2765–2775, 2018.
- [8] C. Wang, N. Gao, J. Wang, N. Jia, T. Bi, and K. Martin, "Robust operation of a water-energy nexus: A multi-energy perspective," *IEEE Transactions* on Sustainable Energy, vol. 11, no. 4, pp. 2698–2712, 2020.
- [9] J. Zhong, Y. Li, Y. Cao, Y. Tan, Y. Peng, Y. Zhou, Y. Nakanishi, and Z. Li, "Robust coordinated optimization with adaptive uncertainty set for a multienergy microgrid," *IEEE Transactions on Sustainable Energy*, vol. 14, no. 1, pp. 111–124, 2022.

- [10] Y. Li, Y. Sun, J. Liu, C. Liu, and F. Zhang, "A data driven robust optimization model for scheduling near-zero carbon emission power plant considering the wind power output uncertainties and electricity-carbon market," *Energy*, vol. 279, p. 128053, 2023.
- [11] S. R. Pokhrel, K. Hewage, G. Chhipi-Shrestha, H. Karunathilake, E. Li, and R. Sadiq, "Carbon capturing for emissions reduction at building level: A market assessment from a building management perspective," *Journal of Cleaner Production*, vol. 294, p. 126323, 2021.
- [12] F. B. Salamah, "Building-integrated carbon capture: A study on the design and potential of carbon emission offsets from buildings," Ph.D. dissertation, Arizona State University, 2021.
- [13] V. S. Tabar, M. T. Hagh, and M. A. Jirdehi, "Achieving a nearly zero energy structure by a novel framework including energy recovery and conversion, carbon capture and demand response," *Energy and Buildings*, vol. 230, p. 110563, 2021.
- [14] D. R. Liyanage, K. Hewage, H. Karunathilake, and R. Sadiq, "Feasibility of carbon-capturing in building heating systems: A life cycle thinkingbased approach," *International Journal of Greenhouse Gas Control*, vol. 132, p. 104056, 2024.
- [15] (2017) Local businesses capture emissions and save FortisBC energy through pilot program. [Online]. Available: https://www.fortisbc.com/news-events/media-centredetails/2017/11/20/20171120-Local-businesses-capture-emissions-andsave-energy-through-FortisBC-pilot-program
- [16] (2024) Carbon Capture Pilot Program. [Online]. Available: https://www.fortisbc.com/services/sustainable-energyoptions/carbon-capture-pilot-program
- [17] (2023) Carbon capture reduces greenhouse gas emissions and saves money for Surrey school. [Online]. Available: https://www.fortisbc.com/newsevents/media-centre-details/2023/04/04/carbon-capture-reducesgreenhouse-gas-emissions-and-saves-money-for-surrey-school
- [18] (2024) CarbonQuest. [Online]. Available: https://carbonquest.com/building-carbon-capture/how-it-works
- [19] (2024) Carbon capture technology for sustainable communities. [Online]. Available: https://carbonquest.com/building-carbon-capture
- [20] (2024) NYC Multifamily Developer Taps CarbonQuest to Reduce Emissions. [Online]. Available: https://carbonquest.com/projects/1930broadway
- [21] (2023) NYC skyscrapers turning to carbon capture to lessen climate change. [Online]. Available: https://phys.org/news/2023-05-nycskyscrapers-carbon-capture-lessen.htmlgoogle_vignette
- [22] (2023) The US Section 45Q Tax Credit for Carbon Oxide Sequestration: An Update . [Online]. Available: https://www.globalccsinstitute.com/wp-content/uploads/2020/04/45Q_Brief_in_template_LLB.pdf
- [23] (2023) CCS in Europe regional overview. [Online]. Available: https://www.globalccsinstitute.com/wp-content/uploads/2023/11/CCS-in-Europe-Regional-Overview-Global-CCS-Institute-pdf.pdf
- [24] (2023) What is The 45Q Tax Credit? [Online]. Available: https://carbonherald.com/what-is-45q-tax-credit/
- [25] Y. Li, Y. Zou, Y. Tan, Y. Cao, X. Liu, M. Shahidehpour, S. Tian, and F. Bu, "Optimal stochastic operation of integrated low-carbon electric power, natural gas, and heat delivery system," *IEEE Transactions on Sustainable Energy*, vol. 9, no. 1, pp. 273–283, 2017.
- [26] M. Xiao and G. F. Smaisim, "Joint chance-constrained multi-objective optimal function of multi-energy microgrid containing energy storages and carbon recycling system," *Journal of Energy Storage*, vol. 55, no. 11, p. 105842, November 2022.
- [27] Q. Wu and C. Li, "Modeling and operation optimization of hydrogen-based integrated energy system with refined power-to-gas and carbon-capturestorage technologies under carbon trading," *Energy*, vol. 270, no. 9, p. 126832, May 2023.
- [28] J. Woo, R. Fatima, C. J. Kibert, R. E. Newman, Y. Tian, and R. S. Srinivasan, "Applying blockchain technology for building energy performance measurement, reporting, and verification (mrv) and the carbon credit market: A review of the literature," *Building and Environment*, vol. 205, p. 108199, 2021.
- [29] C. Shao, C. Feng, M. Shahidehpour, Q. Zhou, X. Wang, and X. Wang, "Optimal stochastic operation of integrated electric power and renewable energy with vehicle-based hydrogen energy system," *IEEE Transactions* on *Power Systems*, vol. 36, no. 5, pp. 4310–4321, September 2021.
- [30] H. Zhang, J. Wang, X. Zhao, J. Yang *et al.*, "Modeling a hydrogen-based sustainable multi-carrier energy system using a multi-objective optimization considering embedded joint chance constraints," *Energy*, vol. 278, no. 17, p. 127643, September 2023.
- [31] Y. Li, F. Zhang, Y. Li, and Y. Wang, "An improved two-stage robust optimization model for cchp-p2g microgrid system considering multienergy operation under wind power outputs uncertainties," *Energy*, vol. 223, no. 10, p. 120048, May 2021.

- [32] M. Yan, N. Zhang, X. Ai, M. Shahidehpour, C. Kang, and J. Wen, "Robust two-stage regional-district scheduling of multi-carrier energy systems with a large penetration of wind power," *IEEE Transactions on Sustainable Energy*, vol. 10, no. 3, pp. 1227–1239, 2018.
- [33] H. Huang, Z. Li, L. M. I. Sampath, J. Yang, H. D. Nguyen, H. B. Gooi, R. Liang, and D. Gong, "Blockchain-enabled carbon and energy trading for network-constrained coal mines with uncertainties," *IEEE Transactions* on Sustainable Energy, vol. 14, no. 3, pp. 634 – 1647, 2023.
- [34] G. Chen, H. Zhang, H. Hui, and Y. Song, "Fast wasserstein-distance-based distributionally robust chance-constrained power dispatch for multi-zone hvac systems," *IEEE Transactions on Smart Grid*, vol. 12, no. 5, pp. 4016– 4028, 2021.
- [35] L. J. Hong, Z. Huang, and H. Lam, "Learning-based robust optimization: Procedures and statistical guarantees," *Management Science*, vol. 67, no. 6, pp. 3447–3467, December 2021.
- [36] X. Zhang and D. Wang, "A gnn-based day ahead carbon intensity forecasting model for cross-border power grids," in *Proceedings of the* 14th ACM International Conference on Future Energy Systems, 2023, pp. 361–373.
- [37] (2023) California Independent System Operator. [Online]. Available: https://www.caiso.com/Pages/default.aspx
- [38] (2023) Electricity Maps. [Online]. Available: https://www.electricitymaps.com/
- [39] (2023) WattTime. [Online]. Available: https://www.watttime.org/
- [40] D. Bertsimas, V. Gupta, and N. Kallus, "Data-driven robust optimization," *Mathematical Programming*, vol. 167, pp. 235–292, 2018.
- [41] G. Sun, C. Jiang, X. Wang, and X. Yang, "Short-term building load forecast based on a data-mining feature selection and lstm-rnn method," *IEEJ Transactions on Electrical and Electronic Engineering*, vol. 15, no. 7, pp. 1002–1010, July 2020.
- [42] D. Maji, P. Shenoy, and R. K. Sitaraman, "Carboncast: multi-day forecasting of grid carbon intensity," in *Proceedings of the 9th ACM International Conference on Systems for Energy-Efficient Buildings, Cities, and Transportation*, Boston, Massachusetts, USA, November 2022, pp. 198–207.
- [43] A. Ben-Tal, L. El Ghaoui, and A. Nemirovski, *Robust optimization*. Princeton university press, 2009, vol. 28.
- [44] MCE Community Choice Energy . (2023) MCE Light Green Non-Residential Rates. [Online]. Available: https://www.mcecleanenergy.org/wp-content/uploads/2023/07/MCE-Commercial-Rates_07282023.pdf
- [45] The National Renewable Energy Laboratory . End Use Load Profiles for the U.S. Building Stock. [Online]. Available: https://www.nrel.gov/buildings/end-use-load-profiles.html
- [46] Rockafellar, Uryasev, Nemirovsky, and Shapiro. (2023) Chance constrained optimization. [Online]. Available: https://web.stanford.edu/class/ee364a/lectures/chance_constr.pdf
- [47] G. C. Calafiore and M. C. Campi, "The scenario approach to robust control design," *IEEE Transactions on automatic control*, vol. 51, no. 5, pp. 742– 753, May 2006.
- [48] G. C. Calafiore and L. E. Ghaoui, "On distributionally robust chance-constrained linear programs," *Journal of Optimization Theory and Applications*, vol. 130, no. 4, pp. 1–22, December 2006.
- [49] J. González-Sopeña, V. Pakrashi, and B. Ghosh, "An overview of performance evaluation metrics for short-term statistical wind power forecasting," *Renewable and Sustainable Energy Reviews*, vol. 138, 2021.
- [50] L. Alvarado-Barrios, A. R. del Nozal, J. B. Valerino, I. G. Vera, and J. L. Martínez-Ramos, "Stochastic unit commitment in microgrids: Influence of the load forecasting error and the availability of energy storage," *Renewable Energy*, vol. 146, pp. 2060–2069, 2020.
- [51] A. Mobasseri, M. Tostado-Véliz, A. A. Ghadimi, M. R. Miveh, and F. Jurado, "Multi-energy microgrid optimal operation with integrated power to gas technology considering uncertainties," *Journal of Cleaner Production*, vol. 333, no. 4, p. 130174, January 2022.
- [52] R. Kruse, S. Mostaghim, C. Borgelt, C. Braune, and M. Steinbrecher, "Multi-layer perceptrons," in *Computational intelligence: a methodologi*cal introduction. Springer, 2022, pp. 53–124.



Yijie Yang (Graduate Student Member, IEEE) is a Ph.D. student at the Department of Computing, The Hong Kong Polytechnic University, Hong Kong, advised by Professor Dan Wang. Ms. Yang received her bachelor's and master's degrees from the Faculty of Computing, Harbin Institute of Technology, Harbin, in 2020 and 2022, respectively. Her current research focuses on data-driven low-carbon operation of energy systems under uncertainty.



Jian Shi (M'15-SM'19) is an Assistant Professor in the Department of Engineering Technology and Department of Electrical and Computer Engineering at the University of Houston. He received his Ph.D. in Electrical and Computer Engineering in 2014 at Mississippi State University. His research interests include deep decarbonization of the electric energy grid, low-/zero-carbon energy hubs, maritime transportation electrification, and energy equity and justice. Dr. Shi has received multiple awards and recognitions, including the NSF CAREER Award (2024), UTC Emerging

Leaders (Cohort of 2024), Early-Career Research Fellowship from the National Academies of Sciences, Engineering and Medicine (NASEM-GRP, 2024), and Faculty Research Excellence Award at UH (2022).



Zhu Han (S'01–M'04-SM'09-F'14) received the B.S. degree in electronic engineering from Tsinghua University, in 1997, and the M.S. and Ph.D. degrees in electrical and computer engineering from the University of Maryland, College Park, in 1999 and 2003, respectively.

From 2000 to 2002, he was an R&D Engineer of JDSU, Germantown, Maryland. From 2003 to 2006, he was a Research Associate at the University of Maryland. From 2006 to 2008, he was an assistant professor at Boise State University, Idaho. Currently, he is a John

and Rebecca Moores Professor in the Electrical and Computer Engineering Department as well as in the Computer Science Department at the University of Houston, Texas. Dr. Han's main research targets on the novel game-theory related concepts critical to enabling efficient and distributive use of wireless networks with limited resources. His other research interests include wireless resource allocation and management, wireless communications and networking, quantum computing, data science, smart grid, security and privacy. Dr. Han received an NSF Career Award in 2010, the Fred W. Ellersick Prize of the IEEE Communication Society in 2011, the EURASIP Best Paper Award for the Journal on Advances in Signal Processing in 2015, IEEE Leonard G. Abraham Prize in the field of Communications Systems (best paper award in IEEE JSAC) in 2016, and several best paper awards in IEEE conferences. Dr. Han was an IEEE Communications Society Distinguished Lecturer from 2015-2018, AAAS fellow since 2019, and ACM distinguished Member since 2019. Dr. Han is a 1% highly cited researcher since 2017 according to Web of Science. Dr. Han is also the winner of the 2021 IEEE Kiyo Tomiyasu Award, for outstanding early to mid-career contributions to technologies holding the promise of innovative applications, with the following citation: "for contributions to game theory and distributed management of autonomous communication networks."



Chenye Wu (Senior Member, IEEE) received the Ph.D. degree from the Institute for Interdisciplinary Information Sciences (IIIS), Tsinghua University, Beijing, China, in July 2013. He is currently an Assistant Professor at the School of Science and Engineering, The Chinese University of Hong Kong, Shenzhen, China. Before joining CUHK Shenzhen, he was an Assistant Professor at IIIS, Tsinghua University. He was with ETH Zurich as a Wiss. Mitarbeiter (Research Scientist), working with Prof. Gabriela Hug, in 2016. Before that, Prof. Kameshwar Poolla and the late Prof.

Pravin Varaiya hosted him as a postdoctoral researcher at the University of California Berkeley, Berkeley, CA, USA, for two years. During 2013-2014, he spent one year with Carnegie Mellon University, Pittsburgh, PA, USA, as a Postdoc Fellow, hosted by Prof. Gabriela Hug and Prof. Soummya Kar.

He is currently working on economic analysis, optimal control and operation of power systems. His Ph.D. advisor is Prof. Andrew Yao, the laureate of the A.M. Turing Award in the year of 2000. He was the co-recipient of the Best Paper Award of IEEE SmartGridComm 2012, IEEE PES General Meeting 2013, and IEEE PES General Meeting 2020.



Dan Wang is a professor in the Department of Computing, The Hong Kong Polytechnic University. His research interests lie in computer networking and recently in smart energy systems. He published in ACM eEnergy and ACM Buildsys, and he won the best papers in both conferences. He is currently the steering committee chair of ACM eEnergy. He is an advisor of EMSD, the Hong Kong SAR government. He has extensive experience in applied research and his research results have been adopted by industry, including Huawei, IBM, Henderson, etc.